12th International Conference on Fracture Mechanics of Concrete and Concrete Structures
FraMCoS-12
B.L.A. Pichler, Ch. Hellmich, P. Preinstorfer (Eds)

https://doi.org/10.21012/FC12.1141
MS03-3:1

VOIDS DETECTION IN BONDED METAL/COMPOSITE OR CONCRETE/COMPOSITE ASSEMBLIES USING ACOUSTO-ULTRASONIC METHOD: CONTRIBUTION OF SIMULATION

AURELIEN DOITRAND[*], CHEIKH A. T. SARR[†], SYLVAIN CHATAIGNER[†], LAURENT GAILLET[†] AND NATHALIE GODIN[*]

[*] INSA Lyon, University Claude Bernard Lyon 1, CNRS, MATEIS, UMR5510,
69621 Villeurbanne, France
e-mail: nathalie.godin@insa-lyon.fr, aurelien.doitrand@insa-lyon.fr

[†] University Gustave Eiffel, IFSTTAR, SMC, MAST, Route de Bouaye, F-44341 Bouguenais, France
e-mail: sylvain.chataigner@univ-eiffel.fr ; laurent.gaillet@univ-eiffel.fr

Key words: Acousto-ultrasonic, Acoustic Emission, Bonded assemblies, Defects, FEM model.

Abstract:
The present work aims at studying voids detection in bonded metal/composite or concrete/composite assemblies using numerical simulations of Acousto-Ultrasonic (AU). The assemblies are made of a steel or concrete substrate and a unidirectional composite laminate bonded with an epoxy adhesive. This study allows assessing experimentally and numerically the sensitivity of AU technique to voids within the joint. Three-dimensional FE models are developed to simulate the influence of voids and sensor location on the recorded signal. Both the relative location of the sensor with respect to the defect epicentre and the kind of receiver sensor are thus fundamental for defect detection. The proposed model enables determining the parameters affected by the size of the defect (such as e.g., amplitude and frequency centroid) and an analysis based on the relevant parameters increases the probability of detection of voids.

1 INTRODUCTION

Adhesively bonded composite reinforcements have been increasingly used in civil engineering. Used in the repair, reinforcement and rehabilitation of structures with composites, they extend the service life of structures. Despite their advantages, the effectiveness of bonded joints can be compromised due to the presence of adhesion defects or damage such as voids, porosity, poor adhesion or low cohesion strength. It is necessary to provide methods to detect and/or identify defects present in the bonded joints. It requires reliable and robust control and monitoring methods to check the quality of the assemblies produced and monitor their progress over time. This should be able to discriminate the different types of defects that may be encountered and evaluate their severity. Defects need to be identified either during initial control or inspection during service life. The acousto-ultrasonic (AU)

technique shows good potential to answer this challenge [1-7]. It is a combination of ultrasonic characterization and acoustic emission.

The aim of our study is to evaluate the potential of the AU technique for detecting and identifying defects such as voids encountered in bonded civil engineering assemblies [8-10]. AU is a non-destructive testing technique that combines acoustic emission (AE) and ultrasound (US) techniques. It involves sending an elastic wave through a material using piezoelectric transducers and then, after it has propagated, receiving it for processing using AE methods. The resulting stress wave is then analysed using acoustic emission methodology through the description of related signal parameters. There are still challenges in applying AU method on these structures with several layers of dissimilar materials. This method, as the standard guided ultrasonic inspection method, is based on the interaction of the waves with the defects present in the adhesive joint. The main difference is that the wave modes and propagation paths are not well established. The signal is therefore difficult to analyse; nevertheless, it is a rich source of information that reflects the material properties, microstructure and possible presence of defects. The signals are reflected by different layers and overlapped, scattered and attenuated. A single experimental approach is thus not sufficient to fully understand this interaction. In this context, the numerical simulation of the test will be useful.

We begin this paper by describing the characteristics of the studied assemblies and the measurement protocol. Then, we present the results obtained in terms of repeatability, detection capability and the identification of simulated defects. The last part is dedicated to the modelling aspect.

2 SPECIMENS/ AU MEASUREMENTS

In this part, we present measurements obtained on assemblies of pultruded carbon fibre composite plates bonded to steel or concrete substrates [8]. The composite (T800 S carbon fibre and epoxy matrix) and the dimensions of the adhesive layers are 300 mm x 50 mm and 1.4 mm and 1 mm thick respectively. The composites are bonded to steel plates (S355, dimension 320 mm x 100 mm, 5 mm thick) or concrete slabs (C25/30, dimension 410 mm x 210 mm, 110 mm thick). The used adhesive is a Sikadur30 two-component cold-curing epoxy resin. The surface preparations are the following: sandblasting and degreasing of the surfaces, followed by light abrasion and degreasing of the composite reinforcement. The reference sample is named type α. For samples with voids named type-β, a type β_1 defect is simulated with a lack of adhesive on a central area and a type β_2 defect corresponds to a lack of adhesive on 1/3 of the bonded area in the center of the joint (Table 1).

AU equipment from MISTRAS Group is used: an ARB1410 electronic card for transmission and a PCI2 card for reception. A preliminary study enabled to select the sensors and the coupling method. We used a S9204 sensor for transmission and two R15 sensors for reception (Figure 1). These piezoelectric sensors have a resonance frequency around 150 kHz and are coupled to the samples with phenyl salicylate, a crystal with a T_F= 40°C that solidifies at room temperature.

Table 1: Characteristics of the specimens with sizes of the voids. CC: Concrete and Composite, SC: Steel and Composite, α for the specimen with no defect in the adhesive joint and β for the specimens with voids defects.

CC or SC -α	**reference sample**
CC-β_1	centered void : 100 mm x 50 mm dimension
CC-β_2	centered void : 1/3 of the bonded surface
SC-β_1	centered void : 50 mm x 25 mm dimension
SC-β_2:	centered void : 1/3 of the bonded surface

Independent series of measurements

(including the decoupling/coupling of the sensors) are performed on each sample for both types of assembly. 7 measurements containing 10 shots are carried out for each sample, giving a total of 70 emitted signals. The emitted signal is a continuous square wave with a frequency of 150 kHz and an amplitude that varied according to the type of assembly (4 V for steel-composite S-C assemblies, 10 V for concrete-composite C-C assemblies). First investigations allowed validating the repeatability of the procedure through the determination of time-domain cross-correlation coefficients between signals received from the same test specimen [8].

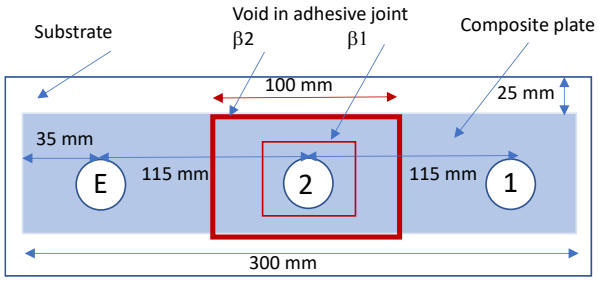

Figure 1: Sensors locations on specimen and position of the defect for SC specimen. The sensor N°2 is located above the defect at 115 mm from the emitter, while the N°1 is at 230 mm away from the emitter.

3 EXPERIMENTAL RESULTS

To assess the voids detection ability, a parametric analysis is conducted by comparing several acoustic emission parameters of the received signals for all samples. Figures 2 and 3 show the energy values represented by the signal strength recorded for the healthy α sample and β samples. A significant difference is observed for the sensor located at the epicenter of the defect (sensor 2). On the contrary, for sensor 1, there is little difference between the reference material α sample and the β samples whatever the type of substrate. The location of the sensor with respect to the defect location seems accordingly to be of primary importance for a robust defect detection. Morover, the size of the defect does not seem to have a significant influence on the features calculated at the epicenter of the defect. With a Principal Component Analysis (PCA), that considers all AE features recorded (such as rise time, amplitude, frequency centroid, energy, duration, …..) a separation exists between the signals collected on the α-type samples and the samples with defects mainly for the data collected in position 2. Nevertheless, for the sensor position N°1, test specimens with defects seem to be also distinguished from the reference one.

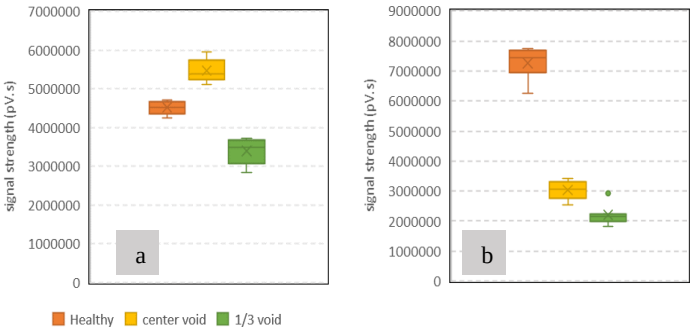

Figure 2: Signal strength of AE signals received in concrete-composite assemblies: a) sensor N°1 b) sensor N°2

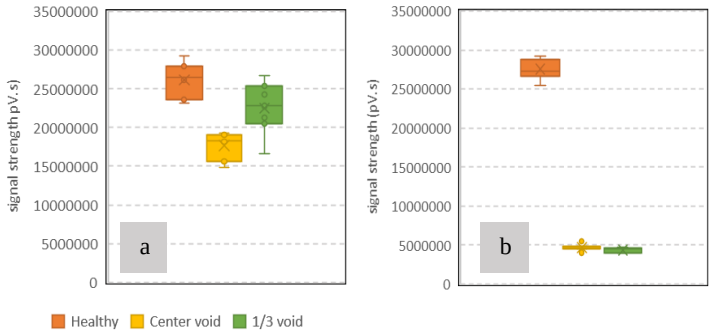

Figure 3: Signal strength of AE signals received in steel-composite assemblies: a) sensor N°1 b) sensor N°2

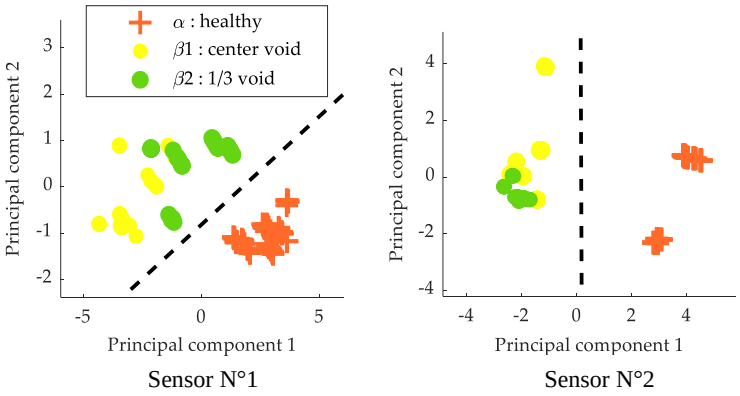

Figure 4. First principal component as a function of second principal component for SC-α sample, β_1 and β_2 samples obtained with a) only sensor N°1 data and b) only sensor N°2 data.

4 MODELLING OF THE AU

4.1 Model

A 3D FE model [9] is produced using Abaqus commercial software (Dassault Systèmes Simulia Corp., Providence, RI, USA). The geometry consists of a steel substrate with a composite plate using an epoxy adhesive, as shown in Figure 1. We simulate three models, one without defects and two with voids of different sizes in the middle of the assembly. The assembly is modelled by three layers corresponding to the steel substrate, the composite plate and the epoxy joint. The behavior of each layer is assumed to be linear elastic. The excitation is simulated by an imposed displacement at one of the mesh nodes corresponding to the emitting sensor (E) center location. The input signal is defined as a 150 kHz sinusoidal signal (Figure 5). Material damping is described using Rayleigh coefficients α and β [11]. Two kinds of sensors are simulated: a perfect point-sensor denoted PS and a R15 sensor. The ideal "point sensor" is a virtual sensor that would acquire signals at a single measurement point (at a node) without sensor effects. The radius of a piezoelectric ceramic for the R15 sensor is equal to 7.25 mm, so the aperture effect that results in a non-uniform response over its entire active surface is considered and its frequency response [12]. The velocity is calculated by considering the average out-of-plane velocity weighted over the sensor's surface and the sensitivity function of the sensor. In this study, the coupling effect is not considered. All numerical signals are filtered with a Butterworth filter from 20 kHz to 1200 kHz. In order to compare the experimental signals and the numerical signals, the end of the experimentally acquired signals is determined using an energy criterion [13]. For each point in the waveform, the cumulative energy calculated from the beginning is compared with the energy contained in a 10 µs window following that point. If this energy is less than a certain threshold (0.1 %) of the cumulative energy, then the corresponding point is considered to be the end of the signal.

The main extracted features analyzed are the following: signal amplitude, duration, centroid frequency and the peak frequency. Additional less conventional features have been calculated, such as the opening frequency (5% of the energy of the spectrum) or the cut-off frequency (95 % of energy).

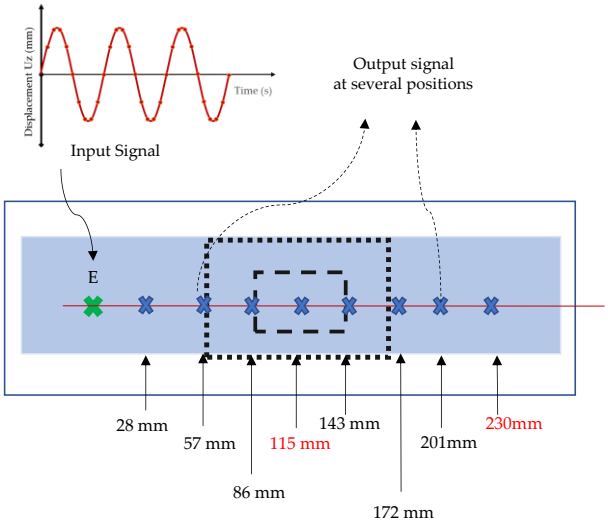

Figure 5: Simulation of the AU test indicating the location of the virtual transmitter and receiver sensors, each virtual receiver is separated by about 28 mm.

4.2 Results

Figure 6 shows the variation of amplitude as a function of the distance between the emitter (E) and the receiver. The data collected by the ideal "point sensor" (PS) or obtained by the R15 sensor are represented for the reference assembly and for the type-β assemblies. We can observe with the perfect sensor a significant decrease in the amplitude at the epicenter of the defect, more important for the larger void size β_2. The characteristics of the signals received after the void are significantly equivalent to those of the reference. Simulation with the ideal "point sensor" highlights the difficulty of detecting the void for a sensor not located at the void epicenter. The variation in frequency features as a function of distance from the transmitter is shown in Figure 7. There is a significant decrease in the frequency content of the signal recorded with the ideal "point sensor" just above the defect. Frequencies around 150 kHz

are attenuated compared with lower frequencies. The reduction in frequency content changes with the size of the defect. Indeed, the frequency barycenter is less than 100 kHz for the β_2 type defect and greater than 100 kHz for the smallest β_1 defect.

Indeed, in a healthy sample for the sensor in position 2, 78% of the spectral energy is in the 125-200 kHz frequency range, whereas it is only 53% for the β_1 defect and 17% for the β_2 defect. The change in this frequency content can be correlated to the size of the void. At the sensor location 230 mm after the defect, no significant difference is observed. It can be seen that the size of the void has an influence on the signature of the AU signal recorded by the sensors at the epicenter of the void and could be distinguished with the ideal "point sensor".

In application, we should find the same result with broadband sensors, which should not modify the frequency content.

Using the R15 sensor, we can observe a change in the frequency barycenter, although the differences are much less marked (Figure 7b). The R15 sensor amplified the frequency content around 150 kHz due to its resonance and eliminated this reduction in frequency content even for sensor 2. The energy contained in the 125–200 kHz frequency band is 91% and 87%, respectively, for the undamaged sample and the sample containing a β1-type defect. Separation from the undamaged material was therefore difficult, and the probability of detection decreased. Taking the R15 sensor into account also reduces the probability of detecting voids in the frequency domain compared with the ideal " point sensor".

Nevertheless, the simulation shows that certain descriptors are little affected by the sensor effect, such as the opening frequency, and retain a good sensitivity to the defect and its size (Figure 8). Simulation can be used to determine the relevant features that are sensitive to the size of the detect, even with the sensor effect.

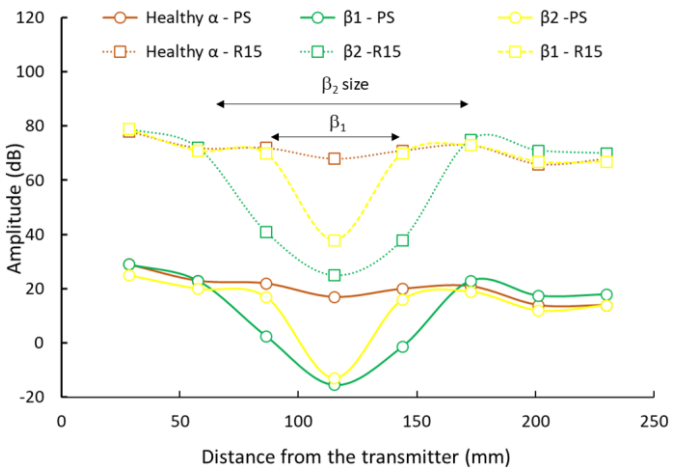

Figure 6: Variation of amplitude as a function of the distance between the emitter and the ideal "point sensor" (PS, o) or R15 (□) for the different assemblies.

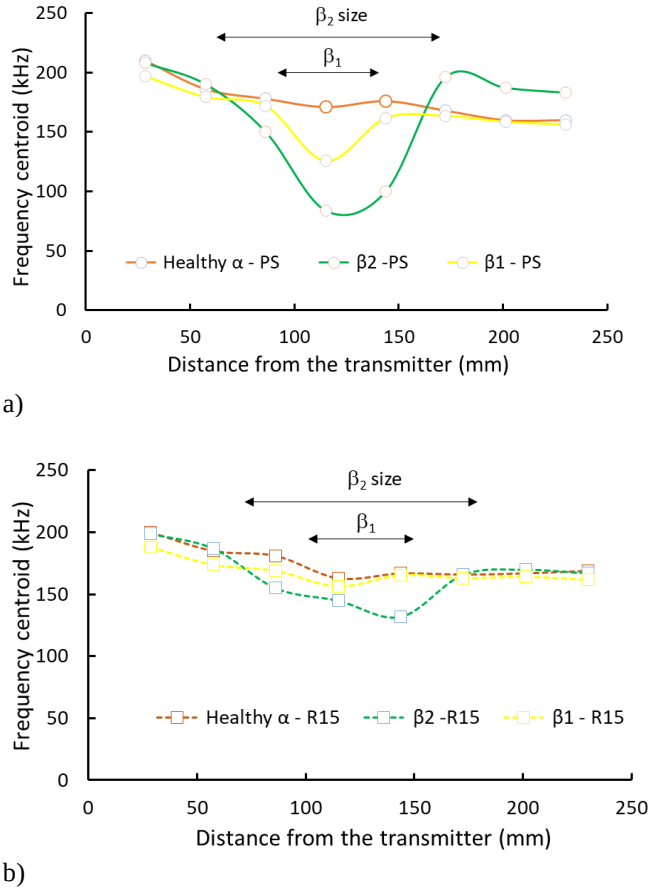

Figure 7: Variation of frequency barycenter as a function of the distance between the emitter and a) the ideal "point sensor" (PS, o) or b) R15 (□) for the different assemblies.

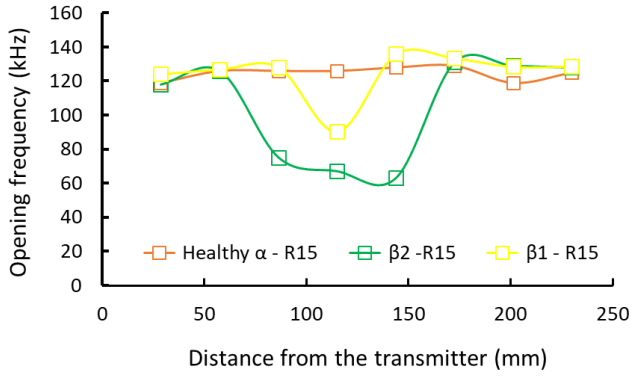

Figure 7: Variation of opening frequency as a function of the distance between the emitter and the R15 sensor (□) for the different assemblies.

7 CONCLUSION

We have observed that the position of the receiving sensor is crucial for the detection of bonding defects using the acousto-ultrasonic method. The time and frequency features of the signals acquired by the receiver sensor are strongly influenced by the presence of a void in relation to a healthy sample mainly if the receiver sensor is located at the epicenter of the defect. Features such as amplitude, energy, frequency barycenter and peak frequency are more affected as the size of the void increases. This effect is attenuated when a R15 sensor is considered, particularly for the smallest defect size. These results highlight the difficulty of using only AE features (parameters extracted from the recorded signals) which reduce the characteristics of the signal to just a few parameters, some of which become too imprecise for void detection when the sensitivity of a real R15-type sensor is added. This modelling is not exhaustive and does not consider all the aspects interacting with the signal (emitting sensor, coupling, acquisition system). Nevertheless, this study has highlighted the potential offered by the numerical approach for a better understanding of wave propagation in the assembly and its interaction with defects, as well as its usefulness for an optimal choice of receiving sensors and relevant features.

REFERENCES

[1] R. D. Adams and P. Cawley, “A review of defect types and nondestructive testing techniques for composites and bonded joints,” NDT International, vol. 21, no. 4, pp. 208-222, 1988.

[2] A. Vary, “Acousto-Ultrasonic Characterization of Fiber Reinforced Composites,” chez Officie of Naval Research Conference, Cambridge, Massachusetts, 1981.

[3] V. K. Srivastava, “Acousto-ultrasonic evaluation of interface bond strength of coated glass fibre-reinforced epoxy resin composites,” Composite Structures, vol. 30, pp. 281-285, 1995.

[4] S. Tanary, M. Haddad, A. Fahr and S. Lee, Nondestructive Evaluation of Adhesively Bonded Joints in Graphite/Epoxy Composites Using Acousto-Ultrasonics, Journal of Pressure Vessel Technology, vol. 114, no. 3, pp. 344 - 352, 1992.

[5] O. Y. Kwon and S. H. Lee, “Acousto-ultrasonic evaluation of adhesively bonded CFRP-aluminum joints,” NDT & E In-ternational, vol. 32, no. 3, pp. 153-160, 1999.

[6] V. Janapati, F. Kopsaftopoulos , F. Li , S. Jun Lee , F-K. Chang, “Damage Detection Sensitivity Characterization of Acousto-Ultrasound-based SHM Techniques”, Structural Health Monitoring, Vol. 15(2), pp. 143-161, 2016.

[7] C. Barile, C. Casavola et G. Pappalettera, “Acousto-ultrasonic evaluation of interlaminar strength on CFRP laminates,” Composite Structures, vol. 208, pp. 796 - 805, 2019.

[8] Sarr, C.A.T.; Chataigner, S.; Gaillet, L.; Godin, N. Nondestructive evaluation of FRP-reinforced structures bonded joints using acousto-ultrasonic: Towards diagnostic of damage state. Constr. Build. Mater. 2021, 313, 125499.

[9] Guo, J.; Doitrand, A.; Sarr, C.; Chataigner, S.; Gaillet, L.; Godin, N. Numerical voids detection in bonded

metal/composite assemblies using acousto-ultrasonic method. Appl. Sci. 2022, 12, 4153.

[10] Sarr, C. A., Chataigner, S., Gaillet, L., & Godin, N. (2022). Defects Detection and Identification in Adhesively Bonded Joints between CFRP Laminate and Reinforced Concrete Beam Using Acousto-Ultrasonic Technique. Journal of Composites Science, 6(11).

[11] Z. Hamam, N. Godin, P. Reynaud, C. Fusco, N. Carrère, and A. Doitrand, "Transverse cracking induced acoustic emission in carbon fiber-epoxy matrix composite laminates", Materials, vol. 15, 394, 2022.

[12] S. Dia, T. Monnier, N. Godin and F. Zhang, "Primary Calibration of Acoustic Emission Sensors by the Method of Reciprocity, Theoretical and Experimental Considerations", Journal of Acoustic Emission, vol. 30, pp. 152-166, 2012.

[13] N. Morizet, N. Godin, J. Tang, E. Maillet, M. Fregonese and B. Normand, "Classification of acoustic emission signals using wavelets and Random Forests: Application to localized corrosion," Mechanical systems and signals processing, Vols. 70-71, pp. 1026-1037, 2019.